J 7

RADIATIVE HEAT TRANSFER IN CURVED SPECULAR SURFACES IN CZOCHRALSKI CRYSTAL GROWTH FURNACE

Zhixiong Guo and Shigenao Maruyama
Institute of Fluid Science, Tohoku University, Aoba-ku, Katahira 2-1-1, Sendai 980, Japan

Takao Tsukada
Institute for Chemical Reaction Science, Tohoku University, Aoba-ku, Katahira 2-1-1, Sendai 980, Japan

A numerical investigation of radiative heat transfer constructed by curved surfaces with specular and diffuse reflection components is carried out. The ray tracing method is adopted for the calculation of view factors, in which a new ray emission model is proposed. The second-degree radiation ring elements are introduced, which are of engineering importance and numerical efficiency. The accuracy of the method is analyzed and verified using a simple configuration. The present computation using the proposed ray emission model is in good agreement with the analytical solution. As a numerical example and engineering application, the effects of the specular reflection and the meniscus of the melt surface in Czochralski (CZ) crystal growth are investigated. A marked temperature decrease in the melt surface is found by introducing specular reflection and the meniscus. The combined effects of the specular reflection and the meniscus should be considered in precision heat transfer control of a CZ apparatus.

INTRODUCTION

Much attention has been paid to radiative heat exchange of Czochralski (CZ) crystal growth furnaces in recent decades in the demand for precision heat transfer control of CZ growth. It is known that radiation is a dominant mechanism for heat transfer in the CZ crystal growth apparatus [1–3]. The surface of the melt is specular and curved in CZ silicon crystal growth. A perusal of the relevant literature reveals, however, that most existing investigations are applicable only when the surfaces are diffuse and simple geometries.

Analytical solutions have been utilized in analyzing radiation transfer with specular components. As Modest [4] and Maruyama [5] point out, however, such methods are limited to simple geometries. A recent numerical study by one of the present authors [6] was concerned with surfaces that possess both specular and/or

Received 13 May 1997; accepted 7 June 1997.

Part of this work is the result of "Technology for Production of High Quality Crystal," which is supported by the New Energy and Industrial Technology Development Organization (NEDO) through the Japan Space Utilization Promotion Center (JSUP) in the program of the Ministry of International Trade and Industry (MITI) of Japan.

Address correspondence to Professor Shigenao Maruyama, Institute of Fluid Science, Tohoku University, Aoba-ku, Katahira 2-1-1, Sendai 980, Japan. E-mail: maruyama@ifs.tohoku.ac.jp

Numerical Heat Transfer, Part A, 32:595–611, 1997

1040–7782/97 $12.00 + .00

NOMENCLATURE

a, b	half length of the axes of ellipsoid	T_i	surface temperature of A_i
A_i	surface element or area of the element	x, y, z	Cartesian coordinates
$F_{i,j}$	view factor from element A_i to A_j	α, ϵ	absorptivity and emissivity, respectively
$F_{i,j}^A$	absorption view factor, Eq. (2)	θ	polar angle measured from normal vector of a surface
$F_{i,j}^D$	diffuse reflection view factor, Eq. (3)	ρ	reflectivity
$\mathbf{F}$	view factor matrix	σ	Stefan-Boltzmann constant
G_i	irradiance	ϕ	circumferential angle
$\mathbf{I}$	unit matrix	ω	solid angle
J_{Di}	diffuse radiosity, Eq. (4)		
M	number of radiation elements in an enclosure	**Subscripts**	
$2n$	ray partition number parameter, Eq. (16)	a	analytic values
n_θ, n_ϕ	partition number in θ and ϕ directons, respectively	J	values due to diffuse radiosity
N	total number of ray partitions	i, j	values on surfaces A_i and A_j
q_i	heat flux at element A_i	T, X	values due to thermal emission and net heat generation
Q_T	heat transfer rate of emission	**Superscripts**	
Q_X	net rate of heat generation		
$\mathbf{Q}$	heat transfer rate vector	A	absorption
r	radius	D	diffuse reflection
s	distance between disk and ellipsoid	S	specular reflection

diffuse reflectance components in a simple CZ configuration, in which curved surfaces are modeled by numerous linear ring elements. A ray tracing method has been proposed and shown to have advantages for estimating the absorption and diffuse reflection view factors between three-dimensional arbitrary surfaces [5–7]. This concept of view factors has been extended to a radiation element method [8, 9], REM^2, which can treat absorbing, emitting, and scattering media and specular/diffuse surfaces of three-dimensional arbitrary configurations. Hayasaka et al. [10] demonstrated that use of the ray tracing method results in substantial savings in CPU time compared with the Monte Carlo method.

In CZ crystal growth the melt surface forms a meniscus at the crystal-melt contact due to capillary effects. Therefore the melt surface has a steep curvature near the crystal and tends to be flat near the crucible. This meniscus may result in significant radial heat loss from the melt to the surrounding environment, near the crystal-melt interface, and leads to an increased pulling rate compared to the case of a flat surface [11]. In order to evaluate the influence of the meniscus on heat transfer, radiation in complicated curved surfaces of second degree with specular and diffuse reflections should be taken into account. The present investigation addresses this problem. A literature survey reveals that no publication is available that involves the present aspect.

The computation accuracy and CPU time of the ray tracing method depend on its ray emission model. An effective ray emission model cannot only improve the accuracy, but can also speed up the calculation. A new ray emission model is proposed in the present study, which improves the accuracy from $(2n)^{-1}$ to n^{-2}

compared with the previous model used by Maruyama [5] and Maruyama and Aihara [6]. Here, $2n$ is the ray partition number parameter. Also, the CPU time can be substantially decreased.

In the present treatise the ray tracing method is employed for radiation heat transfer based on the new ray emission model. Special considerations are given to specular and diffuse reflections between curved surfaces of second degree. The accuracy of computation of view factors and radiation heat transfer by the new ray emission model is examined using a simple configuration. Radiative heat transfer in a complicated CZ crystal growth system is demonstrated as a numerical example and engineering application. The effects of the specular reflection and the meniscus of the melt surface on radiation heat transfer in the CZ growth are scrutinized.

METHOD OF ANALYSIS

Definition of View Factors

It is generally known that radiation transport between a gray diffusely emitting element and any receiving element can be described conveniently by a configuration factor, or view factor, in terms of a geometric function of each element. As Modest [4] mentioned, however, difficulties arise in calculating configuration factors when specular reflection in curved surfaces is concerned. In particular, in complicated systems such as CZ crystal growth furnace, it is very difficult to obtain the specular view factors. Maruyama [5] introduced new definitions of absorption and diffuse reflection view factors for analyzing specular and/or diffuse surfaces. These view factors can be calculated with ease by numerical approaches. The absorption view factor $F_{i,j}^{A}$ and the diffuse reflection view factor $F_{i,j}^{D}$ are introduced as follows: $F_{i,j}^{A}$ is the fraction of the radiation leaving surface element A_i that is absorbed by surface element A_j; and $F_{i,j}^{D}$, the fraction of the radiation leaving surface element A_i that is diffusely reflected by surface element A_j. A specular fraction is not added to the absorption and diffuse reflection view factors, since it is either absorbed or diffusely reflected by other surfaces after several specular reflections.

Under the assumptions that (1) each surface element has constant temperature, heat flux, and emissivity over the surface element; (2) the surface is gray; (3) the reflectivity and emissivity of a surface element are independent of the incident angle, the radiative properties are of the form [4]

$$\rho = \rho^S + \rho^D = 1 - \alpha = 1 - \epsilon \tag{1}$$

where ρ^S and ρ^D are the specular and diffuse components of the reflectivity, respectively.

The definitions of $F_{i,j}^{A}$ and $F_{i,j}^{D}$ can be formulated as

$$F_{i,j}^{A} = \frac{1}{\pi A_i} \int_{A_i} \int_{2\pi} f_i^j(\theta, \phi)\epsilon_j \cos\theta \, d\omega \, dA_i \tag{2}$$

$$F_{i,j}^{D} = \frac{1}{\pi A_i} \int_{A_i} \int_{2\pi} f_i^j(\theta, \phi)\rho_j^D \cos\theta \, d\omega \, dA_i \tag{3}$$

where $\int_{2\pi} d\omega$ represents integration over the hemispherical solid angle and $f_i^j(\theta, \phi)$ represents the fraction of the ray emitted from dA_i in the direction of (θ, ϕ) that is intercepted by A_j.

Ray Tracing Method

Recent progress in computer graphics has accelerated improvement in the ray tracing method for visualizing calculated data [12, 13]. The ray tracing method is employed in the present calculations of absorption and diffuse reflection view factors. The processes of ray tracing are described in the following.

1. When the ray emitted from element A_i strikes the surface A_j, the intensity I of the ray is divided into the absorbed fraction ΔI^A, diffusely reflected fraction ΔI^D, and specularly reflected fraction ΔI^S in accordance with Eq. (1).
2. Then ΔI^A and ΔI^D are added to $F_{i,j}^A$ and $F_{i,j}^D$, respectively, and the reflected ray with intensity ΔI^S is traced again.
3. When the reflected ray strikes the surface $A_{j'}$, the absorbed and diffusely reflected portions are added to $F_{i,j'}^A$ and $F_{i,j'}^D$, respectively, and the specular fraction is traced again until the ray is attenuated to less than 1% of its initial intensity or is absorbed completely.

After tracing the rays from all the elements, $F_{i,j}^A$ and $F_{i,j}^D$ can be attained automatically. It should be noted that the specular fraction of the ray carries with it the information of the intensity and the element i from which the ray was originally emitted; however, the ray is oblivious to the procedure concerning from which element the ray was reflected.

Radiation Exchange

For analyzing radiation heat exchange, a diffuse radiosity J_{Di} is written as

$$J_{Di} \equiv \epsilon_i \sigma T_i^4 + \rho_i^D G_i \tag{4}$$

where G_i is the irradiance on surface A_i. The diffuse radiation heat transfer rate Q_{Ji} and the net rate of heat generation Q_{Xi} on surface A_i are expressed as

$$Q_{Ji} = A_i(\epsilon_i \sigma T_i^4 + \rho_i^D G_i) \qquad Q_{Xi} = A_i \epsilon_i (\sigma T_i^4 - G_i) \tag{5}$$

When $Q_{Xi} > 0$, the net rate of heat leaves the surface A_i. In an enclosure system composed of M surface element, the irradiation energy and absorption energy of element A_i can be expressed as

$$A_i \rho_i^D G_i = \sum_{j=1}^{M} F_{j,i}^D Q_{Jj} \qquad A_i \epsilon_i G_i = \sum_{j=1}^{M} F_{j,i}^A Q_{Jj} \tag{6}$$

Therefore Eq. (5) can be rewritten as

$$Q_{Ji} = Q_{Ti} + \sum_{j=1}^{M} F_{j,i}^{D} Q_{Jj} \qquad Q_{Xi} = Q_{Ti} - \sum_{j=1}^{M} F_{j,i}^{A} Q_{Jj} \tag{7}$$

in which $Q_{Ti} = A_i \epsilon_i \sigma T_i^4$.

Substituting matrix $\mathbf{F}$ and vector $\mathbf{Q}$ for $F_{j,i}$ and Q_i, respectively, and eliminating Q_{Ji} from Eq. (7), the following relationship is achieved:

$$\mathbf{F}_X \mathbf{Q}_T = \mathbf{I}\mathbf{Q}_X \tag{8}$$

where

$$\mathbf{F}_X = \mathbf{I} - \mathbf{F}^A(\mathbf{I} - \mathbf{F}^D)^{-1} \tag{9}$$

and $\mathbf{I}$ and $(\ )^{-1}$ stand for unit matrix and inverse matrix, respectively. When each element in the enclosure system is specified temperature T_i or heat flux q_{Xi}, the unknown components of q_{Xi} and T_i can be calculated by matrix operation of Eq. (8). The solution becomes purely algebraic. The conventional algebraic tools for matrix operation can be easily applied to the present computation.

RAY EMISSION MODEL

Ray Emission Direction

A ray emission model was used by Maruyama [5] and Maruyama and Aihara [6]. The radiation energy emitted was divided into $(1 + n_\theta n_\phi)$ bundles of rays whose initial intensity is $I = 1/(1 + n_\theta n_\phi)$. The initial direction (θ, ϕ) of the ray was expressed as

$$\begin{aligned} \theta_0 &= \phi_0 = 0 \\ \theta_i &= \left\{ \sin^{-1}\left[(1 + in_\phi - n_\phi)/(n_\phi n_\theta + 1)\right]^{0.5} \right. \\ &\qquad \left. + \sin^{-1}\left[(1 + in_\phi)/(n_\phi n_\theta + 1)\right]^{0.5} \right\}/2 \\ \phi_j &= 2\pi(j - 1)/n_\phi \qquad i \neq 0 \qquad j \neq 0 \end{aligned} \tag{10}$$

A schematic diagram of the ray emission directions is shown in Figure 1. In the above model the θ direction was divided into n_θ levels as shown on the right-hand side of Figure 1*a*, while n_ϕ levels were in the ϕ direction, as displayed in Figure 1*b*. In other words, there were n_ϕ rays emitted from each level of θ direction, and n_θ rays from each level of ϕ direction. Since each ray has equal weight as $1/(1 + n_\theta n_\phi)$, the level weights in θ and ϕ directions are $n_\phi/(1 + n_\theta n_\phi)$ and $n_\theta/(1 + n_\theta n_\phi)$, respectively. The total weight of all rays is unity. Between two adjacent ray emission levels, there is a blind area. If any surface happens to be put

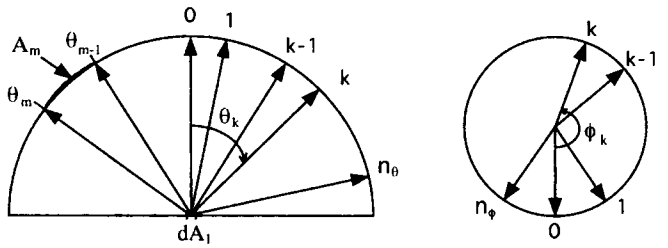

(*a*) (*b*)

Figure 1. Schematic diagram of ray emission directions: (*a*) θ direction and (*b*) ϕ direction.

inside the blind area, no ray will be received by this surface. The error of ray emission direction is then introduced, and it is equal to the level weight. When $n_\theta n_\phi \gg 1$, the error in the direction of θ is n_θ^{-1}, and the error in the direction of ϕ is n_ϕ^{-1}.

The accuracy of ray tracing method is mainly determined by the error of ray emission model. In order to construct a new model of high accuracy, the unit sphere method to calculate or experimentally determine view factors between one infinitesimal and one finite area [4, 14] is referred to. Considering a unit hemisphere as shown in the left-hand side of Figure 1*a*, if θ_{m-1} and θ_m are the start and end polar angles of a finite area A_m, the view factor between dA_1 and A_m can be expressed as [4]

$$F_{d1,m} = \sin^2 \theta_m - \sin^2 \theta_{m-1} \tag{11}$$

View factor $F_{d1,m}$ represents the fraction of diffuse energy leaving dA_1 that is intercepted by A_m. In contrast, it also means the fraction of diffuse energy leaving dA_1 emitted from the θ direction with angle ψ_{m-1}, which satisfies the following relation:

$$\sin^2 \psi_{m-1} = (\sin^2 \theta_m + \sin^2 \theta_{m-1})/2 \tag{12}$$

The level weight P_m in the θ direction is therefore constructed as

$$P_m = F_{d1,m} = \sin^2 \theta_m - \sin^2 \theta_{m-1} \tag{13}$$

If the unit hemisphere is divided into n levels, then

$$\sum_{m=1}^{n} P_m = \sum_{m=1}^{n} F_{d1,m} = 1 \tag{14}$$

Hence the emitted energy is automatically conserved.

Fiveland [15] insisted that equal-weight quadrature has a useful property, in that there are no directional biases in the weights. An equal-level-weight model is

highly required. In addition, to avoid directional biases in the ϕ direction, symmetric weights are desired that are invarient to 90° rotations. The new ray emission directions are proposed as follows:

$$\theta_0 = \phi_0 = 0$$

$$\theta_m = \sin^{-1}\left[\sin^2 \psi_{m-1} + 2/N\right]^{0.5} \qquad m = 1,2,\ldots,n^2 \tag{15}$$

$$\phi_{in+j+1} = (i + nj)\pi/(2n^2) \qquad i = 0,1,\ldots,n-1 \qquad j = 0,1,\ldots,n-1$$

where

$$N = 1 + (2n)^2 \tag{16}$$

$$\psi_0 = \sin^{-1}(1/N)^{0.5} \tag{17}$$

$$\psi_m = \sin^{-1}\left[4/N + \sin^2 \psi_{m-1}\right]^{0.5} \qquad m = 1,2,\ldots,n^2 \tag{18}$$

in which N was the total number of rays and the initial intensity of each ray was $I = 1/N$. The ray emitting directions were arranged on n^2 and N levels relative to the θ and ϕ directions, respectively, as illustrated in Figure 2 in the case of $2n = 6$. In each level of θ direction, there were four rays, so that the symmetric biases were ingeniously avoided. In particular, the level error in the ϕ direction was theoretically the smallest because the ϕ direction was divided into N levels, i.e., the ϕ values of all emitted rays were different. The level errors of the new ray emission model are $4/N$ and $1/N$ in the θ and ϕ directions, respectively. Thus the accuracy of the new model is $4/N = 4/[1 + (2n)^2]$. The new model can be characterized by ray partition number parameter $2n$. When $2n \geq 10$, the accuracy is approximately expressed as n^{-2}. Comparing with the accuracy of $(2n)^{-1}$ in the previous $n_\theta n_\phi$ model when $2n = n_\theta = n_\phi$, the computation accuracy is considerably improved.

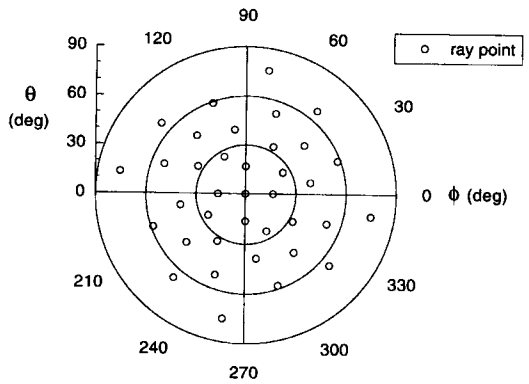

Figure 2. Ray emission directions of new ray emission model when $2n = 6$.

Ray Emission Position and Radiation Elements

The accuracy of view factor calculation by the ray tracing method is also affected by the ray emission positions. In the present investigation with application to CZ crystal growth, an axisymmetric system is taken into account. A diagram of the analysis model of arbitrary surfaces and emission of radiation is portrayed in Figure 3. Arbitrary bodies consist of numerous ring elements i ($i = 1, 2, \ldots, M$). In the previous work [6], only linear ring elements consisting of a part of a circular disc, cylinder, and cone were considered. In the present work, radiation elements composed of curved surfaces of second degree such as a sphere, ellipsoid, and hyperboloid are also introduced. The surface equation with respect to a rectangular system of axes is of the form [16]

$$a(x^2 + y^2) + b(z - c)^2 = d \tag{19}$$

By a suitable choice of parameters a, b, c, and d, surfaces can be constructed. For the linear elements those parameters are

$$\begin{array}{rlll} \text{Disk:} & a = 0 & d = 0 & \\ \text{Cylinder:} & a \neq 0 & b = 0 & \\ \text{Cone:} & d = 0 & a > 0 & b < 0 \end{array} \tag{20}$$

and for second-degree radiation elements, they are

$$\begin{array}{rlll} \text{Sphere:} & a = 1 & b = 1 & d > 0 \\ \text{Ellipsoid:} & a = 1 & b > 0 & d > 0 \\ \text{Hyperboloid:} & a = 1 & b < 0 & d \neq 0 \end{array} \tag{21}$$

Consider a cross section of a ring element in the x-z plane, and let the start and end points of the curve s be s_1 and s_2, respectively. The surface area of the element is calculated as follows:

$$A_i = 2\pi \int_{s_1}^{s_2} x \, ds \tag{22}$$

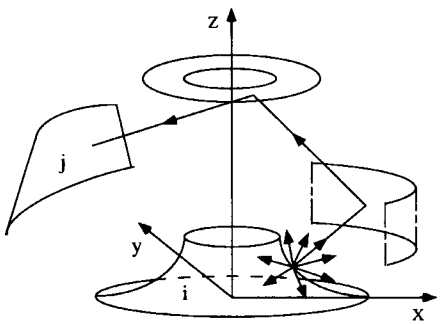

Figure 3. Analysis model of arbitrary surfaces and emission of radiation.

If A_i consists of A_{i1} and A_{i2}, the following relation can be obtained:

$$A_i F_{i,j} = A_{i1} F_{i1,j} + A_{i2} F_{i2,j} \tag{23}$$

Therefore the ray emission position should be located at the surface area center in order to avoid area biases. For axisymmetric surfaces the area center s_c in the x-z plane satisfies the following relation:

$$\int_{s_1}^{s_c} x\,ds = \int_{s_c}^{s_2} x\,ds \tag{24}$$

The new ray emission model is composed of Eqs. (15)–(18) and Eq. (24).

EXAMPLE OF SIMPLE CONFIGURATIONS

The present method for calculating view factors and radiation transfer was first applied to a simple configuration, as depicted in Figure 4. The system consists of a circular disk (A_1) and an ellipsoid (A_2). The geometries of the system are defined by dimensionless parameters A, R, and S:

$$A = a/b \qquad S = s/b \qquad R = r/b \tag{25}$$

in which a, b, r, and s are labeled in Figure 4. In the present study, $A = 0.5$, $R = 1.0$, and $S = 0.5$. The emissivity is assumed to be unity.

The computation of the view factors from ring element ΔA_1 of the disk to ring element ΔA_2 of the ellipsoid or from ΔA_2 to ΔA_1 is performed for various ray partition numbers. The disk is divided into 10 ring elements. Only half of the ellipsoid surface is taken into account, which is in the side near the disk and is also divided into 10 ring elements. Comparisons are made among view factor calculations by the new $2n$ ray emission model and by the $n_\theta n_\phi$ ray emission model [5] and the analysis [17]. The numerical results are evaluated by the following relations:

$$\Delta F_{\Delta 1,\Delta 2} = F_{\Delta 1,\Delta 2} - (F_{\Delta 1,\Delta 2})_a \qquad \Delta F_{\Delta 2,\Delta 1} = F_{\Delta 2,\Delta 1} - (F_{\Delta 2,\Delta 1})_a \tag{26}$$

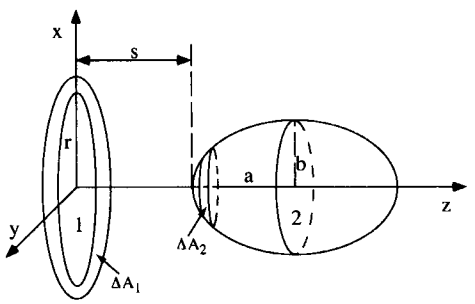

Figure 4. Simple configuration of a disk and an ellipsoid.

where $(F_{\Delta 1,\Delta 2})_a$ and $(F_{\Delta 2,\Delta 1})_a$ are the analytical results based on the analysis of Naraghi and Chung [17]. The comparisons are illustrated in Figure 5 for the case $2n = n_\theta = n_\phi$. The abscissas express the centroid positions of ΔA_1 and ΔA_2 along the nondimensional $X(x/b)$ and $Z(z/b)$ axes in Figures 5*a* and 5*b*, respectively. Subscript $\Delta 2$ in $\Delta F_{\Delta 1,\Delta 2}$ represents the bottom ring element of ΔA_2, which is opposite to the disk, whereas subscript $\Delta 1$ in $\Delta F_{\Delta 2,\Delta 1}$ stands for the central ring element of the disk. The solid symbols are the results of using the $n_\theta n_\phi$ model, and the open symbols are the results of the $2n$ ray emission model. It is seen that, with increase of ray partition parameters $2n$ or $n_\theta n_\phi$, the differences between the calculations and the analyses decrease. Hence increasing the ray emission number will improve computation accuracy. As we know, however, the denser the ray emission, the larger the CPU time. There should be a compromise of the trade-off between accuracy and CPU time. Comparing the results of the $n_\theta n_\phi$ model and the new $2n$ model, the accuracy of the latter model is much higher than that of the former, while the same ray partition number is employed ($2n = n_\theta = n_\phi$). When $2n = 40$, i.e., a total number of $N = 1601$ rays is used, the differences between the analyses and the calculations are within ± 0.01. As expected, the increase of accuracy as well as the decrease of CPU time is achieved by using the new $2n$ ray emission model.

A further comparison of the view factors from ring element to finite area between the simulations by using the $2n$ ray emission model and the analyses [17] is demonstrated in Figure 6. The expressions of $\Delta F_{\Delta 1,2}$ and $\Delta F_{\Delta 2,1}$ are

$$\Delta F_{\Delta 1,2} = F_{\Delta 1,2} - (F_{\Delta 1,2})_a \qquad \Delta F_{\Delta 2,1} = F_{\Delta 2,1} - (F_{\Delta 2,1})_a \tag{27}$$

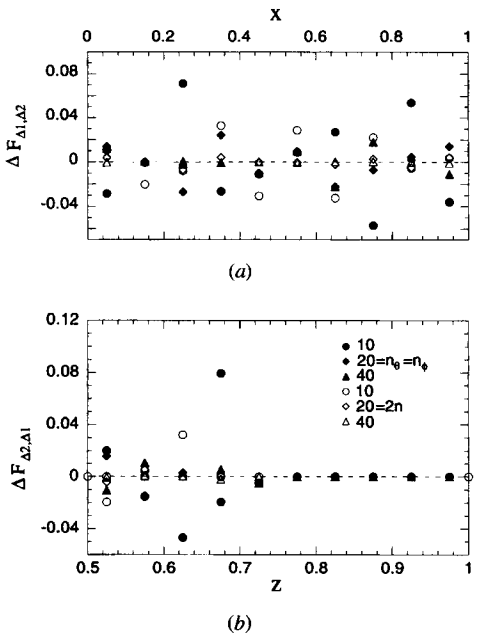

Figure 5. Comparisons of calculation accuracy of view factors from ring element to ring element: (*a*) disk to ellipsoid and (*b*) ellipsoid to disk.

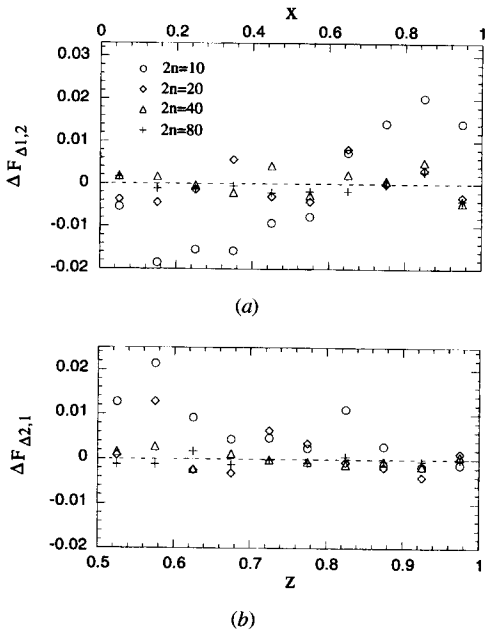

Figure 6. Comparisons of calculation accuracy of view factors from ring element to finite area: (*a*) disk to ellipsoid and (*b*) ellipsoid to disk.

As expected, when the ray partition number increases, the differences between the computations and the analyses decrease. It should be noted that, even in the case of $2n = 20$, the numerical error is in the range of ± 0.01. It is hence expected that the CPU time can be decreased when small partition numbers of ray emission are involved.

To investigate the influence of the element size on the accuracy of the radiation heat exchange, the performance of the total net rate of heat generation of the example system for various ring element numbers N_p is inspected in Figure 7, in which $Q_X = \Sigma Q_{Xi}$. Both the disk and the ellipsoid were divided into N_p elements. As N_p increases, the ring surface element size decreases. Constant temperature (1000 K) is assumed on the surfaces of the disk and ellipsoid. The ambient is assumed to be black at 300 K. The electrical network analogy [4] based on the analytical view factors is utilized to attain the analytical net rate of heat generation Q_{Xa}. As is evident in Figure 7, increasing N_p at the first stage remarkably improves the accuracy of the radiation transfer calculation. However, further increasing N_p after $N_p \geq 8$ is not necessary. When $N_p \geq 8$, the computations are in excellent agreement with analysis solutions.

RADIATION TRANSFER IN CZ FURNACE

As an engineering application, the present numerical model was applied to radiative heat transfer in a Czochralski furnace for silicon crystal growth with diffuse and/or specular surfaces of second degree. The surfaces of silicon crystal and melt are specular against visible light. It can be easily concluded that these surfaces are also specular against larger wavelengths such as infrared thermal

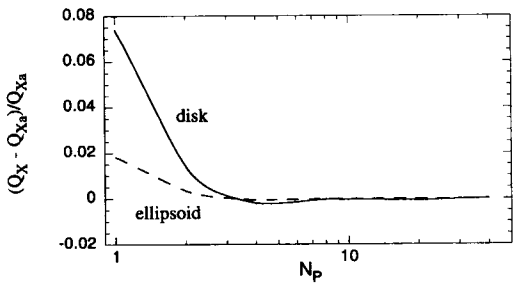

Figure 7. Effect of element size on the radiation heat transfer.

radiation. As has been discussed in the previous work [6], the silicon crystal at high temperatures and the melt are opaque against thermal radiation. Consequently, the silicon crystal and the melt in a CZ furnace are specular against thermal radiation.

The second-degree element is important to describe the meniscus of the melt surface in a CZ furnace. One can approximate the second-degree radiation elements by numerous linear elements. However, the accuracy of the view factors becomes worse when the radiation element is too small and a large number of rays have to be emitted to acquire correct view factors. The use of second-degree elements of appropriate dimension enhances the accuracy and efficiency of the numerical analysis.

The schematic diagram of the CZ furnace with a meniscus is shown in Figure 8*a* [18]. Some important operating parameters and boundary conditions for calculation are given in Table 1. Constant temperatures are applied to the heater, chamber, and shield. In order to examine radiative heat transfer without conduction, the crystal and the metal as well as the crucible, the puller and the supporter are assumed to be adiabatic. The radiation and conduction combined heat transfer can be achieved easily, as shown by Maruyama and Aihara [6]. A radiation surface element division model with 178 ring elements in the CZ furnace is shown in Figure 8*b*. In actual computation, a total of 378 ring elements was used for the radiation heat transfer in the whole CZ growth furnace in the present investigation. For the generation of element coordinate data and the presentation of calculated data, the general-purpose three-dimensional mechanical CAE software PATRAN was employed.

To compare the effects of specular and diffuse reflections, the surfaces of the crystal and the liquid melt are set to be purely diffuse or specular. The chamber is also considered with specular and diffuse surfaces. Other surfaces are all diffuse. Comparison of the surface temperature distributions in the crystal, the melt, and the crucible for two cases of CZ furnace surfaces is demonstrated in Figure 9. It is found that the temperatures on the outer surfaces of the crucible for two cases of CZ furnace surfaces are nearly unchanged. However, the temperatures on the inner surfaces of the crucible for the two cases are different. Marked temperature decreases in the melt and in the crystal areas near the melt were observed when

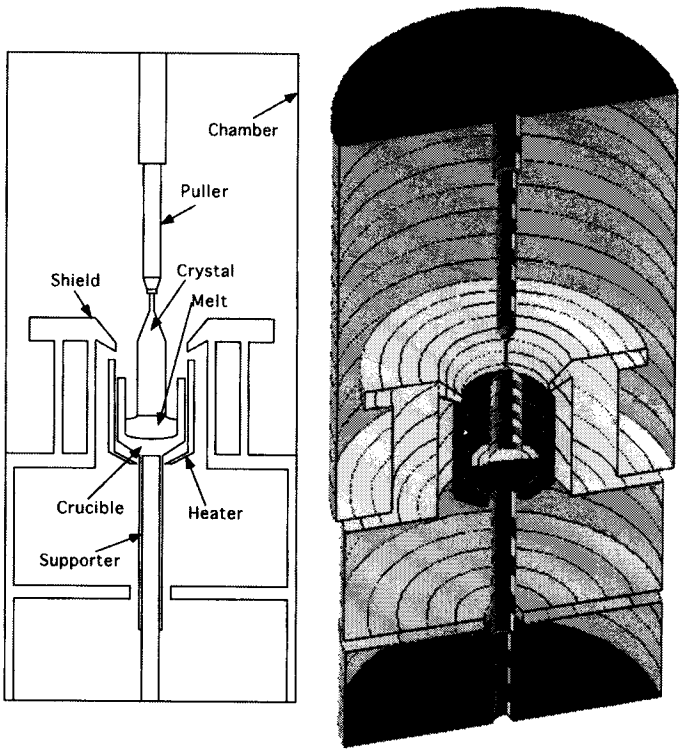

(*a*) (*b*)

Figure 8. (*a*) Model of CZ crystal growth furnace; (*b*) model of CZ ring element division.

the specular surface condition was employed. The effect of specular reflection on temperature decrease is inconsistent with the findings of Maruyama and Aihara [6] for a simple CZ model. However, it should be noted that no temperature difference in the upper areas of the crystal cylinder for various surface conditions was seen in the present complicated CZ furnace. A total of 1601 bundles of ray

Table 1. Operating parameters for CZ silicon calculation

Item	r_i	r_o	ΔH	ϵ	Given T or q
Crucible	36	40.5	96	0.9	0 $W m^{-2}$
Crystal	—	17.5	95	0.55	0 $W m^{-2}$
Melt	—	36	—	0.318	0 $W m^{-2}$
Heater	45.5	53	130	0.9	1700 K
Chamber	180	—	817	0.55	300 K
Puller	—	10	302	0.2	0 $W m^{-2}$
Shield	70	120	476	0.9	1000 K

Here, r_i, inner radius; r_o, outer radius; ΔH, height; unit, millimeters.

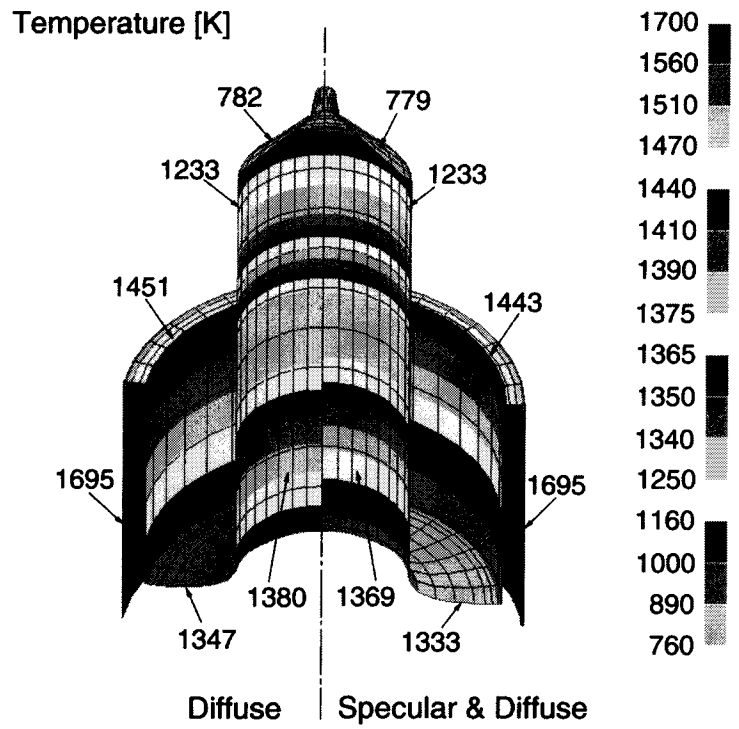

Figure 9. Comparison of temperature distributions in crystal, melt, and crucible for various surfaces of a CZ furnace.

emission ($2n = 40$) was used in the above computations. The calculations were executed on a Sun Ultra-1 (144 MHz) workstation. The CPU time was 1500 s for the case of diffuse surfaces, while 2500 s was spent on the case of specular and diffuse surfaces. For both cases the CPU time on radiation transfer is around 50 s. Most of the CPU time was consumed on the ray tracing method. Thus an effective ray emission model is of significance.

As mentioned in the introduction, the effect of the meniscus of the melt silicon may be of importance in radiation heat transfer in CZ growth. In addition, the influence of specular reflection is more substantial in the melt surface, as seen in Figure 9. A close inspection of the melt temperature is required. A schematic diagram of the meniscus is portrayed in Figure 10*a*, while for comparison, a flat surface is drawn in Figure 10*b*. Comparisons for these two shapes with respect to diffuse and specular surfaces are conducted. In Figure 11 the temperature distributions of the melt surface along the *Xm* direction are depicted for four cases. It is seen that there is a temperature difference between the two shapes of melt surfaces no matter what type of reflection occurs. However, the tendency is different, depending on reflection characters. For diffuse reflection the temperature is larger in the case of the meniscus than in the case of the flat surface, while for specular reflection, the temperature in the case of the meniscus is smaller than

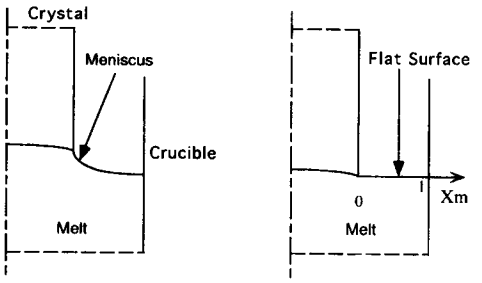

Figure 10. Models of melt surface: (*a*) meniscus and (*b*) flat surface.

that when the meniscus is not considered. The effect of the meniscus is more obvious for a specular surface. In view of the effect of specular reflection, the change of temperature in the melt surface depends on the shape of the melt surface. In the case of the flat surface, the influence of specular reflection is minor. However, when the meniscus is considered, the influence of specular reflection is considerable. The temperature declines about 12 K for the specular meniscus compared with the diffuse meniscus. It can be concluded that the effects of the specular reflection and the meniscus should be taken into account in the precision heat transfer control of a CZ crystal growth furnace.

CONCLUSIONS

Numerical analyses of the ray tracing method were performed to investigate radiative heat transfer among curved surfaces with specular and/or diffuse reflection components. The second-degree radiation ring elements were introduced for analyzing complicated surfaces, which can augment accuracy and efficiency of calculation. The computation errors induced by various ray emission models were analyzed. A new ray emission model was presented. Its higher accuracy was verified by the excellent agreement with analytical solutions for a simple configuration. The

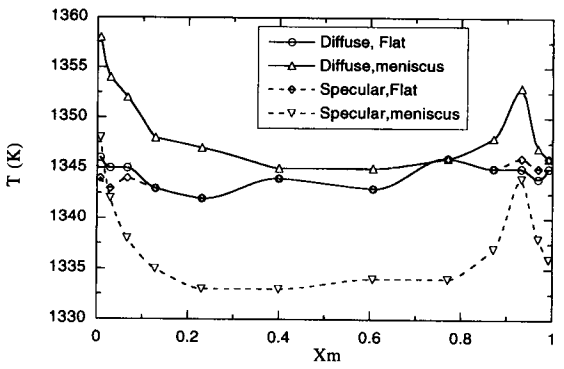

Figure 11. Effects of the meniscus and specular reflection.

CPU time can be substantially decreased by employing the new ray emission model and second-degree ring elements due to the decreases of ray partition number and of radiation ring element number.

The present numerical method was applied to radiation heat transfer in a complicated Czochralski apparatus for silicon crystal growth. The effects of the specular reflection and the meniscus were investigated in detail. A marked temperature decrease in the melt surface was observed for meniscus melt by introducing specular reflection. However, the specular effect is related to the shape of the melt surface. When a flat melt surface was considered, the decrease of temperature was minor. The influence of the meniscus on the temperature profile of the melt surface depended on reflection characteristics. In the case of specular reflection, a decreased temperature distribution in the melt surface occurred for the meniscus surface compared with the flat melt surface, while an increase of temperature for the meniscus surface was observed in the case of diffuse reflection. The combined effects of the specular reflection and the meniscus were significant.

REFERENCES

1. F. Dupret, P. Nicodeme, Y. Ryckmans, P. Wouters, and M. J. Crochet, Global Modelling of Heat Transfer in Crystal Growth Furnaces, *Int. J. Heat Mass Transfer*, vol. 33, pp. 1849–1870, 1990.
2. L. J. Antherton, J. J. Derby, and R. A. Brown, Radiative Heat Exchange in Czocharalski Crystal Growth, *J. Cryst. Growth*, vol. 84, pp. 57–78, 1987.
3. S. Miyahara, S. Kobayashi, T. Fujiwara, T. Kubo, and H. Fujiwara, Global Heat Transfer Model for Czochralski Crystal Growth Based on Diffuse-Gray Radiation, *J. Cryst. Growth*, vol. 99, pp. 696–701, 1990.
4. M. F. Modest, *Radiative Heat Transfer*, chap. 6, McGraw-Hill, New York, 1992.
5. S. Maruyama, Radiation Heat Transfer Between Arbitrary 3-Dimensional Bodies with Specular and Diffuse Surfaces, *Numer. Heat Transfer Part A*, vol. 24, pp. 181–196, 1993.
6. S. Maruyama and T. Aihara, Radiation Heat Transfer of a Czochralski Crystal Growth Furnace with Arbitrary Specular and Diffuse Surfaces, *Int. J. Heat Mass Transfer*, vol. 37, pp. 1723–1731, 1994.
7. S. Maruyama and T. Aihara, Numerical Analysis of Radiative Heat Transfer from Three-Dimensional Bodies with Specular and Diffuse Surfaces, *JSME Int. J.*, vol. 30, pp. 1982–1987, 1987.
8. S. Maruyama and T. Aihara, Radiation Heat Transfer of Arbitrary Three-Dimensional Absorbing, Emitting, and Scattering Media and Specular and Diffuse Surfaces, *Trans. ASME J. Heat Transfer*, vol. 119, pp. 129–136, 1997.
9. S. Maruyama and M. Higano, Radiative Heat Transfer of Torus Plasma in Large Helical Device by Generalized Numerical Method REM^2, *Energy Convers. Manage.*, vol. 38, pp. 1187–1195, 1997.
10. H. Hayasaka, K. Kudo, H. Taniguchi, I. Nakamachi, T. Omori, and T. Katayama, Radiative Heat Transfer Analysis by the Radiation Heat Ray Method (Analysis in a Two-Dimensional Model), *Trans. Jpn. Soc. Mech. Eng.*, vol. 52, no. 476B, pp. 1734–1740, 1986.
11. R. K. Srivastava, P. A. Ramachandran, and M. P. Dudokovic, Radiation View Factors in Czochralski Crystal Growth Apparatus for Short Crystals, *J. Cryst. Growth*, vol. 74, pp. 281–291, 1986.

12. W. T. Welford and R. Winston, *The Optics of Nonimaging Concentrators*, chap. 10, Academic, New York, 1978.
13. S. Maruyama, Uniform Isotropic Emission from an Involute Reflector, *Trans. ASME J. Heat Transfer*, vol. 115, pp. 492–495, 1993.
14. R. Farrel, Determination of Configuration Factors of Irregular Shape, *Trans. ASME J. Heat Transfer*, vol. 98, pp. 311–313, 1976.
15. W. A. Fiveland, The Selection of Discrete Ordinate Quadrature Sets for Anisotropic Scattering, *Fundam. Radiat. Heat Transfer*, HTD-vol. 160, pp. 89–96, 1991.
16. L. Kuipers and R. Timman, *Handbook of Mathematics*, chap. 4, Pergamon, Oxford, 1963.
17. M. H. N. Naraghi and B. T. F. Chung, Radiation Configuration Factors Between Disks and a Class of Axisymmetric Bodies, *Trans. ASME J. Heat Transfer*, vol. 104, pp. 426–431, 1982.
18. K. Kakimoto, P. Nicodeme, M. Lecomte, F. Dupret, and H. J. Crochet, Numerical Simulation of Molten Silicon Flow: Comparison with Experiment, *J. Cryst. Growth*, vol. 114, pp. 715–725, 1991.